International Journal of Bioprinting

RESEARCH ARTICLE

# DLP-printed GelMA-PMAA scaffold for bone regeneration through endochondral ossification

**Jianpeng Gao[1,2†], Hufei Wang[3,4†], Ming Li[1†], Zhongyang Liu[1], Junyao Cheng[1,2], Xiao Liu[1,2], Jianheng Liu[1*], Xing Wang[3,4*], Licheng Zhang[1*]**

[1]Department of Orthopaedics, Chinese PLA General Hospital, 100039 Beijing, China

[2]Medical School of Chinese PLA, 100039 Beijing, China

[3]Beijing National Laboratory for Molecular Sciences, Institute of Chemistry, Chinese Academy of Sciences, 100190 Beijing, China

[4]University of Chinese Academy of Sciences, 100049 Beijing, China

(This article belongs to the *Special Issue: Additive Manufacturing of Functional Biomaterials*)

## Abstract

Intramembranous ossification (IMO) and endochondral ossification (ECO) are two pathways of bone regeneration. The regeneration of most bone, such as limb bone, trunk bone, and skull base bone, mainly occurs in the form of endochondral ossification, which has also become one of the effective ways for bone tissue engineering. In this work, we prepared a well-structured and biocompatible methacrylated gelatin/polymethacrylic acid (GelMA/PMAA) hydrogel by digital light processing (DLP) printing technology, which could effectively chelate iron ions and continuously activate the hypoxia-inducible factor-1 alpha (HIF-1α) signaling pathway to promote the process of endochondral ossification and angiogenesis. The incorporation of PMAA endowed the hydrogel with remarkable viscoelasticity and high efficacy in chelation of iron ions, giving rise to the activation of HIF-1α signaling pathway, improving chondrogenic differentiation in the early stage, and facilitating vascularization in the later stage and bone remodeling. Therefore, the findings have significant implications on DLP printing technology of endochondral osteogenesis induced by the iron-chelating property of biological scaffold, which will provide an effective way in the development of novel bone regeneration.

**Keywords:** Endochondral ossification; Digital light processing; Hydrogel; Bone tissue engineering

†These authors contributed equally to this work.

***Corresponding authors:** Jianheng Liu (jianhengliu@126.com)

Xing Wang (wangxing@iccas.ac.cn)

Licheng Zhang (zhanglcheng301@163.com)

**Citation:** Gao J, Wang H, Li M, *et al*., 2023, DLP-printed GelMA-PMAA scaffold for bone regeneration through endochondral ossification. *Int J Bioprint,* 9(5): 754. https://doi.org/10.18063/ijb.754

**Received:** February 1, 2023
**Accepted:** March 31, 2023
**Published Online:** May 16, 2023



## 1. Introduction

Bone defects caused by various factors such as aging, disease, and trauma are extremely harmful to the body; therefore, effective treatments are necessary to achieve bone tissue repair and regeneration[1, 2]. Intramembranous ossification (IMO) and endochondral ossification (ECO) are two forms of bone regeneration[3-6]. At the bone formation site, vascular hyperplasia leads to an adequate supply of nutrients and oxygen, and the mesenchymal cells can differentiate into osteoblasts, which secrete osteoids and calcify into the bone matrix to form bone tissue [7, 8]. However, intramembranous osteogenesis often results in failure of bone regeneration due to insufficient early angiogenesis[9-11].

Endochondral osteogenesis is the formation of limb bones, trunk bones, skull bones, etc.[12,13]. At the site of long bones, mesenchymal stem cells differentiate into chondrocytes, which secrete cartilage matrix and form cartilage template, followed by vascular invasion, cartilage degeneration, and formation of ossification to complete bone tissue regeneration[10,13,14]. Since the formation of cartilage template and the invasion of blood vessels are two key processes of ECO, if blood vessels fail to regenerate in time after the ECO process is initiated by the chondrogenic differentiation of bone marrow mesenchymal stem cells (BMSCs), ECO is likely to stall in the cartilage template stage, resulting in the failure of osteogenesis[15].

Several pathways have been available to achieve the differentiation of BMSCs to chondrocytes, with HIF-1α-SOX9 being an important one[16-18]. SOX9, a significant regulator of cartilage differentiation, can effectively promote the differentiation and proliferation of chondrocytes[19-22]. Apart from that, hypoxia-inducible factor-1 alpha (HIF-1α) can also encourage the formation of vascular endothelial growth factor (VEGF) to effectively stimulate vascular invasion, timely degeneration of cartilage, and regeneration of bone tissue[23-26]. Therefore, HIF-1α is essential for the process of ECO.

Iron ions and oxygen are known to be two necessary requirements for the degradation of HIF-1α by prolyl hydroxylase domain (PHD). As a consequence, a decrease in the oxygen or iron ion concentration will contribute to a reduced ability of PHD, leading to an increase in HIF-1α[27,28]. In recent years, many researchers have attempted to induce the ECO process by adding desferrioxamine (DFO) to the material[29-31]. As a common iron chelator, DFO can promote the HIF-1α pathway, leading to ECO. However, this exogenous factor will pose a major biosafety risk if the problem of explosive release cannot be solved[32-36]. Therefore, it becomes critical to explore materials to induce the ECO process from their own properties. Sun *et al.* prepared injectable hydrogels that can imitate a hypoxic environment to achieve the regenerated bone defects in rat femoral condyles through ECO using a cell-free and growth factor-free strategy, which is a well-established method to solve bone defects[37]. However, although injectable hydrogels can match defect areas, they are difficult to be prepared directly as pre-designed macroscopic structures. It is therefore essential to use materials with three-dimensional (3D) printing property to fabricate bone tissue engineering scaffolds with desired structures.

Methacrylated gelatin (GelMA) not only has similar biocompatibility to extracellular matrix, but also possesses good photo-crosslinking ability which can achieve liquid-to-solid conversion under ultraviolet (UV) irradiation[38-40]. Numerous scholars have demonstrated that GelMA exhibited certain 3D printing properties to promote the regeneration of bone tissue[41-43]. On the basis of the above materials, in this study, we developed a kind of polymethacrylic acid (PMAA)-modified GelMA/PMAA bio-ink by digital light processing (DLP) printing technique. The carboxyl functional group of PMAA can facilitate the expression of HIF-1α by effectively chelating iron ions; thus, it could significantly promote the chondrogenic differentiation of BMSCs via HIF-1α-SOX9 and the regeneration of blood vessels via HIF-1α-VEGF. Furthermore, the microporous structure of 3D-printed scaffold actively promoted the growth of blood vessels and the regeneration of bone tissue. This has created a promising approach for the treatment of bone defects (Figure 1).

## 2. Materials and methods

### 2.1. Materials

Gelatin from porcine skin was purchased from Sigma-Aldrich, USA. Methacrylic anhydride (MA, 97%) and lithium phenyl-2,4,6-trimethylbenzoyl phosphinate (LAP) were purchased from J&K, China. Methacrylic acid (MAA) was purchased from Aladdin Industrial, China. Cell counting kit-8 (CCK-8), live/dead viability assay kit, and phalloidin were purchased from Beyotime, China.

### 2.2. Preparation of bio-inks

Briefly, gelatin was dissolved in phosphate-buffered saline (PBS) at 50°C under continuous stirring, and MA was added. After reaction in dark for 3 h, the products were diluted with 2× PBS and then dialyzed against distilled water for 5 days at 40°C. The products were then filtered with 0.22-μm paper filter and lyophilized, leading to a white porous foam, before being stored at -20°C for further use.

GelMA and MAA were dissolved in PBS added with LAP (0.25% (w/v)) and tartrazine (0.05% (w/v)), then the bio-inks composed of 15% GelMA/3% PMAA and 15% GelMA/6% PMAA were prepared.

### 2.3. Fabrication of scaffolds

The computer-aided design (CAD) model was designed as a cylinder with interconnected pores, with a diameter of 6 mm, height of 8 mm, and pore size of 600 μm. Then, a DLP printer (BP8601 Pro, EFL, Suzhou, China) was used to prepare the scaffolds, and the parameters were adjusted for printing. Then, the scaffolds were strengthened under UV light for 3 min (Kernel parameters of GelMA scaffold: layer height, 100 μm; light intensity, 10 mW/cm$^2$; exposure time, 15 s; temperature, 29°C. Kernel parameters of GelMA/3% PMAA scaffold: layer height, 100 μm; light intensity, 10 mW/cm$^2$; exposure time, 13 s; temperature,

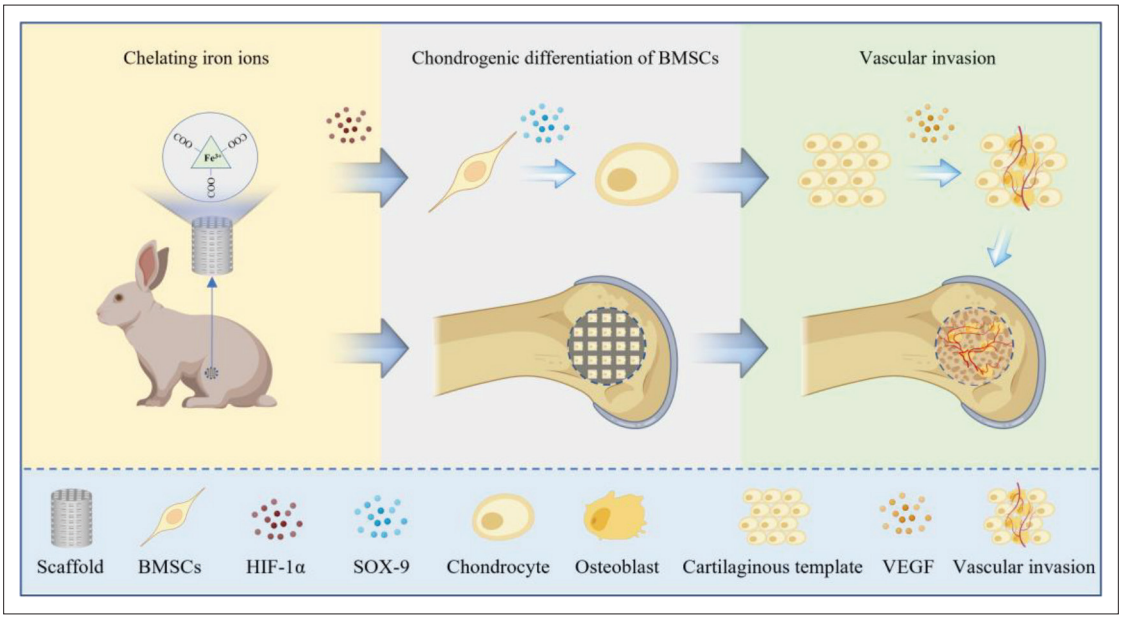


**Figure 1**. Schematic of GelMA/PMAA scaffolds for bone regeneration (ECO). The process of ECO facilitated by scaffolds consists of three key parts: chelation of iron ions, chondrogenic differentiation of BMSCs, and vascular invasion.

29°C. Kernel parameters of GelMA/6% PMAA scaffold: layer height, 100 μm; light intensity, 10 mW/cm$^2$; exposure time, 11 s; temperature, 29°C).

## 2.4. Characterization

### *2.4.1. Nuclear magnetic resonance (NMR)*

After dissolution of GelMA in $D_2O$, the degree of methacryloyl (DS) substitution of GelMA was quantified using $^1$H NMR spectroscopy (400 MHz, Bruker, Germany). An internal reference for the signal with δ = 4.79 ppm was used, and tetramethylsilane (TMS) was used as an internal standard. According to the previous study[44], the degree of substitution (DS) of methacrylate was obtained from the $^1$H NMR spectrum of GelMA and calculated as:

$$DS = \frac{0.3462}{0.0380} \times \frac{I_{5.5ppm}}{I_{1ppm}} \quad (I)$$

### *2.4.2. Fourier transform infrared (FTIR)*

The freeze-dried scaffolds were grinded into powder. Pure gelatin and GelMA powders were used as the control samples. FTIR spectra of the samples were obtained using an FTIR spectrometer (TENSOR-27, Bruker, German) scanned in the frequency range of 4000–500 cm$^{-1}$ at a scanning resolution of 2 cm$^{-1}$ for 32 scans.

### *2.4.3 Microstructure of the 3D-printed hydrogel scaffolds*

The scaffolds were observed using a scanning electron microscope (SEM, HITACHI, SU8100) after lyophilization (Quorum, K850) and gold/palladium sputter coating (HITACHI, MC1000).

### *2.4.4. Compressive tests*

A compression test was performed on a printing scaffold (Φ10 mm × 5 mm) by the universal tensile machine (3365 Instron, USA) at room temperature. For the compression modulus, it was defined as an initial slope of line region of the stress–strain curve. The mechanical indexes (compressive stress and modulus) were acquired according to the software ($n$ = 3).

### *2.4.5. Swelling*

The different scaffolds were placed into PBS and soaked for 24 h at 37°C, and their weights (Ws) were measured after sufficient swelling. Then, the scaffolds were freeze-dried to obtain their dry weight (Wd). The swelling ratio was calculated as:

$$\text{Swelling ratio} = \frac{Ws - Wd}{Wd} \quad (II)$$

### *2.4.6. Degradation*

The different scaffolds were lyophilized, and their weights (W0) were measured. Then, the lyophilized scaffolds were placed in PBS solution and soaked at 37°C. The PBS was changed every 2 days, and the samples were removed on the 1st, 3rd, 5th, 7th, 9th, 12th, 15th, 21th, 27th, 33th, 39th, 45th, 51th, 54th, and 55th days. After rinsing twice with deionized water, the samples were lyophilized and weighed (Wt). The remaining weight was calculated as:

$$\text{Remaining weight}(\%) = \frac{Wt}{W0} \times 100\% \quad (III)$$

#### *2.4.7. Capacity of iron ion adsorption*

The different hydrogels were immersed in 10 mL of $FeCl_3$ and placed on an incubator shaker for 6 h. Afterward, the adsorbent was removed, and the biosorption was calculated to analyze the difference in adsorption capacity by inductive coupled plasma (ICP) emission spectrometer of the different scaffolds.

### 2.5. Cell extraction and culture

The BMSCs and human umbilical vein endothelial cells (HUVECs) used in this experiment were both from the Orthopedic Laboratory of the PLA General Hospital (the ethical number: 2022-x18-51). The original generation of BMSCs was expanded to the third generation with medium containing α-MEM, fetal bovine serum (FBS, 10%), and penicillin–streptomycin (1%) for experiments. The HUVECs were cultured with medium containing high glucose-Dulbecco's Modified Eagle Medium (H-DMEM), FBS (10%), and penicillin–streptomycin (1%). Both types of cells were cultured in this medium—refreshed every 2 days—in a 37°C and 5% $CO_2$ environment.

### 2.6. Cell viability

#### *2.6.1. Extracts of different scaffolds*

The scaffolds were soaked in medium for 48 h at 37°C. For different scaffolds, 100% extracts were prepared according to the standard of 1.25 $cm^2$/mL and diluted to different concentrations of 75%, 50%, and 25%.

#### *2.6.2. CCK-8*

BMSCs were cultured in extracts with different concentrations of different scaffolds for 1–5 days. After the color deepened for 1 h with the addition of CCK-8 (10%), the cell viability was analyzed using a microplate reader (Thermo Fisher, Waltham, MA, USA).

#### *2.6.3. Live/dead staining of cells cultured with extracts*

BMSCs were cultured for 48 h in the extracts at the optimal concentration obtained via the CCK-8 assay. The cells were incubated with live/dead dye for 15 min, and then observed under a fluorescence microscope (Ni-U, Nikon, Tokyo, Japan), where green represented living cells and red represented dead cells.

#### *2.6.4. Phalloidin staining of cells cultured with extracts*

BMSCs cultured for 48 h in the extracts were fixed in 4% paraformaldehyde solution for 30 min. After three washes with PBS, the cells were stained with phalloidin for 30 min and DAPI for 5 min. The morphology of the cytoskeleton was observed with a confocal microscope (Olympus, FV3000, Japan).

#### *2.6.5. Live/dead staining of cells cultured on scaffolds*

Sterile scaffolds were soaked in medium for 15 min in 24-well plates; following their removal from the medium, 1 mL of cell suspension ($5 \times 10^4$ cells) was added. BMSCs were seeded on different scaffolds and cultured in medium for 48 h. The cells were incubated with live/dead dye for 15 min, and then observed under a confocal microscope (Olympus, FV3000, Japan), where green represented living cells and red represented dead cells.

### 2.7. Effect of scaffold on the chondrogenic induction *in vitro*

The experiments in this section were divided into three groups: control, GelMA, and GelMA/3%PMAA groups. All experiments were repeated three times.

#### *2.7.1. Immunofluorescence staining*

After co-culture of BMSCs with different scaffolds in osteogenic induction medium for 5 days, the cells were fixed with 4% paraformaldehyde and permeabilized with 0.1% Triton-X100. Cells were then incubated with primary antibody overnight and secondary antibody for 1 h. Nuclei were then stained with DAPI and washed with PBS three times before observation under a confocal microscope.

#### *2.7.2. Quantitative real-time PCR*

The scaffolds were immersed in the medium for half an hour and then removed from the medium. A total of $10^5$ cells were seeded on the surface of the scaffolds and cultured for 24 h in normal medium, which was then replaced with chondrogenic induction medium (α-MEM, 10% FBS, 2 mg/L insulin, 3 mg/L transferrin, 1 mM pyruvic acid, 10 μg/L TGF-β1, and 100 nM dexamethasone). After 5 days and 10 days of culture, total RNA was extracted from the cells for real-time PCR using Trizol reagent (Servicebio, G3013).

#### *2.7.3. Western blot*

Cells were inoculated onto scaffolds and cultured with chondrogenic induction medium for 5 days before total cellular protein was extracted using Radio Immunoprecipitation Assay (RIPA) lysate (Servicebio, G2002), and protein concentration was then determined using the BCA protein concentration kit (Servicebio, G2026). After passing through the process of sodium dodecyl-sulfate polyacrylamide gel electrophoresis (SDS-PAGE), membrane transfer, immunoblotting, and chemiluminescence detection, the signal intensity was measured using ImageJ software.

### 2.8. Effect of scaffold on the blood vessel regeneration *in vitro*

The experiments in this section were divided into three groups: control, GelMA, and GelMA/3%PMAA groups. All experiments were repeated three times.

#### 2.8.1. Migration experiment using transwell assay

The effect of different scaffolds on the migration of HUVECs through transmembrane was observed using

transwell assay. The scaffolds were placed in 24-well plates and then HUVECs ($10^4$/well) were inoculated in the upper chamber with a pore size of 8 μm and cultured for 12 h and 24 h using low-serum medium (H-DMEM, 2% FBS, 1% penicillin–streptomycin), after which the cells were fixed and the upper layer was removed with cotton swabs, stained with 1% crystalline violet. After staining, the cells were observed under a microscope, and cell detection was performed using ImageJ.

#### *2.8.2. Scratch wound assay*

HUVECs ($10^5$) were inoculated on 6-well plates and cultured to 80%–90% confluence with complete medium (H-DMEM, 10% FBS, 1% penicillin–streptomycin). The cells were scratched with a 1000 μL sterile tip to form straight rows of scars, and then the suspended cells were washed off, the medium was replaced with low-serum medium (H-DMEM, 2% FBS, 1% penicillin–streptomycin), and the culture was continued for 12 h, following which the extent of scratch healing was determined.

#### *2.8.3. Tube formation assay*

In order to explore the ability of different scaffolds to promote angiogenesis, Matrigel (BD, growth factor-reduced, 356231) was covered on the surface of μ-Slide Angiogenesis (ibidi, 81506), and then $10^4$ cells were inoculated on the surface of Matrigel. Different conditioned culture medium was used to induce tubes for 6 h, and they were observed under a microscope. The extent of angiogenesis on the obtained images was determined using ImageJ software.

### 2.9. Effect of scaffold *in vivo*

Eighteen of New Zealand white rabbits (2.5 kg ± 0.5 kg, male) were randomly divided into three groups: blank, GelMA, and GelMA/3%PMAA groups, and each sample was repeated three times. All animals used in this study were obtained from the Animal Experiment Center of the PLA General Hospital and approved by the Ethics Committee (2022-x18-51).

#### *2.9.1. Implantation in rabbit radio defects*

The rabbits were anesthetized, and the distal femur was shaved and disinfected. After cutting the skin and subcutaneous tissue, a cylindrical defect, which was 6 mm in diameter, was created using a surgical drill, without penetrating the contralateral cortex in the distal femur. The sterile scaffolds were inserted into the defect site, and the subcutaneous tissue and skin were sutured layer by layer. The rabbits were sacrificed at week 4 and week 8 post-operatively for the next step of treatment.

#### *2.9.2. Micro-CT analysis*

The Inveron MM System (Siemens, Munich, Germany) was used to evaluate the amount of new bone in each group of rabbits via micro-CT scans. The scanning parameters were an effective pixel size of 17.34 μm, a current of 500 μA, a voltage of 80 kV, and an exposure time of 1500 ms. The two-dimensional (2D) images were reconstructed into 3D images using Inveron Research Workplace (Siemens) to calculate the bone regeneration parameters: bone mineral density (BMD), bone volume/total volume (BV/TV), trabecular thickness (Tb.Th), and trabecular spacing (Tb.Sp).

#### *2.9.3. Histology analysis*

Samples were decalcified in 10% Ethylenediamine Tetraacetic Acid (EDTA), dehydrated in a gradient of ethanol, and cleared using xylene. The samples were then embedded in paraffin and cut into 10-mm slices using a microtome for staining.

### 2.10. Statistical analysis

Statistical analysis was performed by one-way analysis of variance (ANOVA) with *post hoc* tests using the GraphPad Prism software (version 8, GraphPad, USA). The data are expressed as the mean ± standard deviation (SD), and all experiments were performed at least three times. The results were analyzed by one-way ANOVA with the Tukey–Kramer multiple comparison analysis. A value of $p < 0.05$ was regarded as statistically significant ($^*p < 0.05$, $^{**}p < 0.01$, and $^{***}p < 0.001$).

## 3. Results

### 3.1. Characterization and degradation of GelMA/PMAA scaffolds

The mechanical and biological properties of GelMA hydrogels can be regulated by the degree of methacrylate (DS) substitution as well as the concentration and crosslinking time of GelMA. First, we synthesized the macromonomer via methacryloyl (MA) reacting with gelatin (**Figure S1A** in Supplementary File). The local high-resolution $^1$H NMR spectra of gelatin (left) and GelMA (right) in Figure 2A showed the appearance of new proton signals at 5.5 and 5.7 ppm (–CH=$CH_2$) in the macromonomer, suggesting that the methyl acryloyl group was successfully grafted onto the side chain of gelatin. The substitution degree of methacrylate was about 90%, and GelMA with interconnected pores could be easily prepared by exposing it to UV for 10 s (**Figure S1B** and **S1C** in Supplementary File).

To better harmonize the mechanical strengths, we chose PMAA concentrations of 3% and 6% as a way of exploring more suitable concentrations for *in vivo* implantation. The introduction of PMMA increased the toughness and strength of the scaffolds compared to GelMA (Figure 2D). At the same time, the scaffolds' modulus decreased from 66.72 ± 4.73 kPa to 28.42 ± 3.15 kPa with the increase of MAA concentration (Figure 2E). The structure of the scaffolds was observed by SEM, which had a macropore

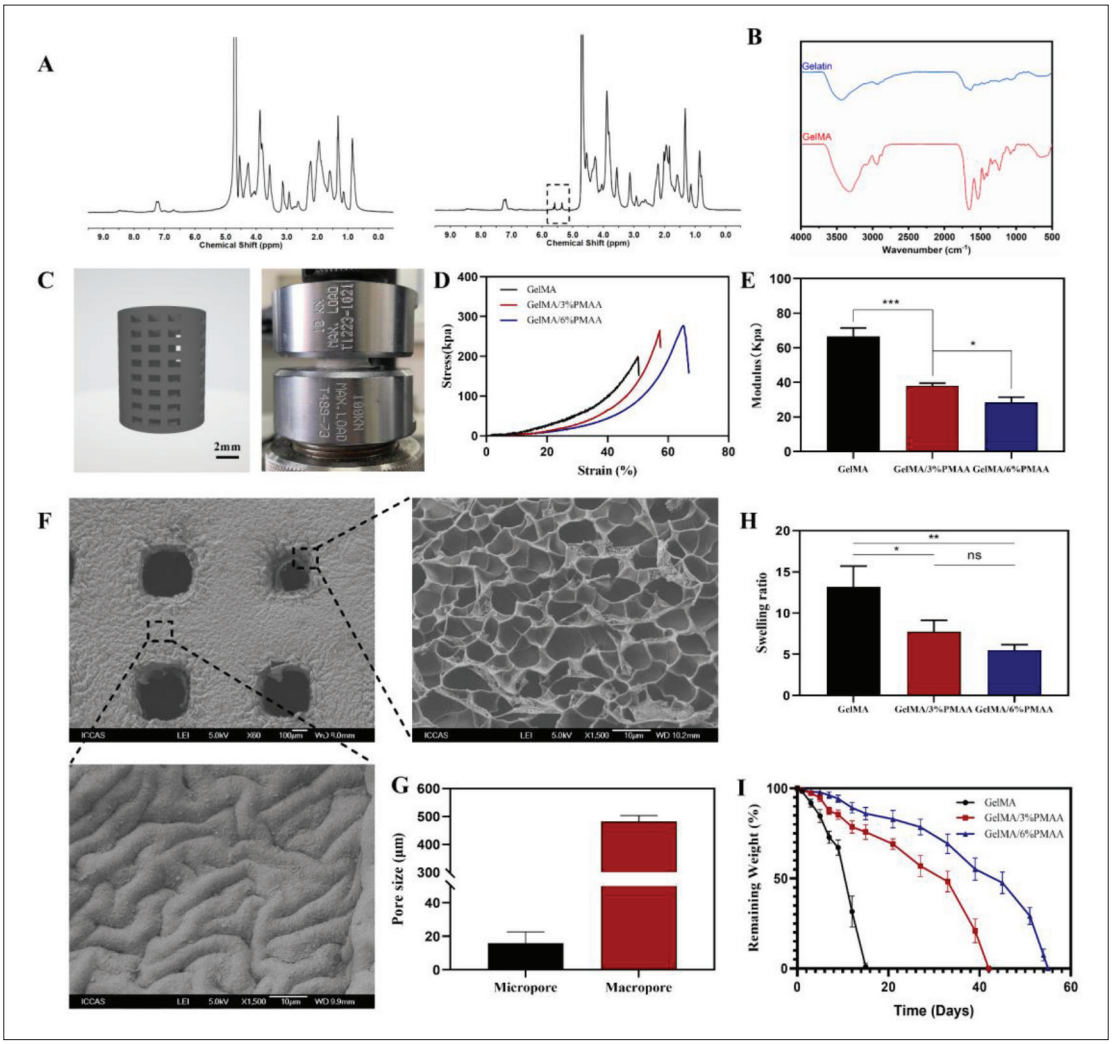


**Figure 2**. Characterization and degradation of GelMA/PMAA scaffolds. (A) $^{1}$H NMR spectra of gelatin (left) and GelMA (right). (B) FTIR spectra of gelatin and GelMA. (C) Images of 3D modeling and compression test of scaffolds. (D) The compressive stress–strain curves of scaffolds. (E) Compressive modulus of scaffolds. (F) SEM image of a 3D-printed scaffold. (G) Pore size of scaffolds. (H) Swelling of different scaffolds. (I) *In vitro* degradation behavior of the three scaffolds in PBS (37°C, pH = 7.4). Data were analyzed via a one-way ANOVA analysis and are shown as mean ± standard deviation (*$p < 0.05$, **$p < 0.01$, ***$p < 0.001$, $n = 3$).

of approximately 500 μm and a micropore of 17 μm inside the scaffolds as well (Figure 2F and G), which facilitated nutrient transport and cell growth. The excellent structure of the scaffolds' macropores and micropores is expected to provide a good basis for vascular regeneration and bone regeneration. The swelling ratios of scaffolds increased with the extension of soaking time and reached the swelling equilibrium after soaking in PBS for 24 h (Figure 2H). The equilibrium swelling ratios of GelMA, GelMA/3% PMAA, and GelMA/6% PMAA scaffolds were 13.21 ± 2.52, 7.74 ± 1.41, and 5.52 ± 0.65, respectively. The swelling ratio of scaffolds decreased dramatically with the increasing weight ratio of PMAA, which could be attributed to the addition of PMAA that increased the crosslinking degree of the scaffold and limited the entry of water. In addition, the degradation time of GelMA/3%PMAA (42 days) and GelMA/6% PMAA (55 days) may be more suitable for bone regeneration than that of the GelMA (15 days, Figure 2I).

### 3.2. Biocompatibility of GelMA/PMAA scaffold

For bone tissue engineering, the basis for clinical application is the availability of good biocompatibility. Different concentrations of extracts (100%, 75%, 50%, 25%) were prepared according to the standards of extract preparation. It was found that GelMA/6% PMAA had a lower optical density (OD) value compared to the others, while GelMA/3%PMAA could promote cell proliferation when the concentration of extract was adjusted to 50% and 25%, which might be related to the different degrees of acidic environment caused by the high concentration

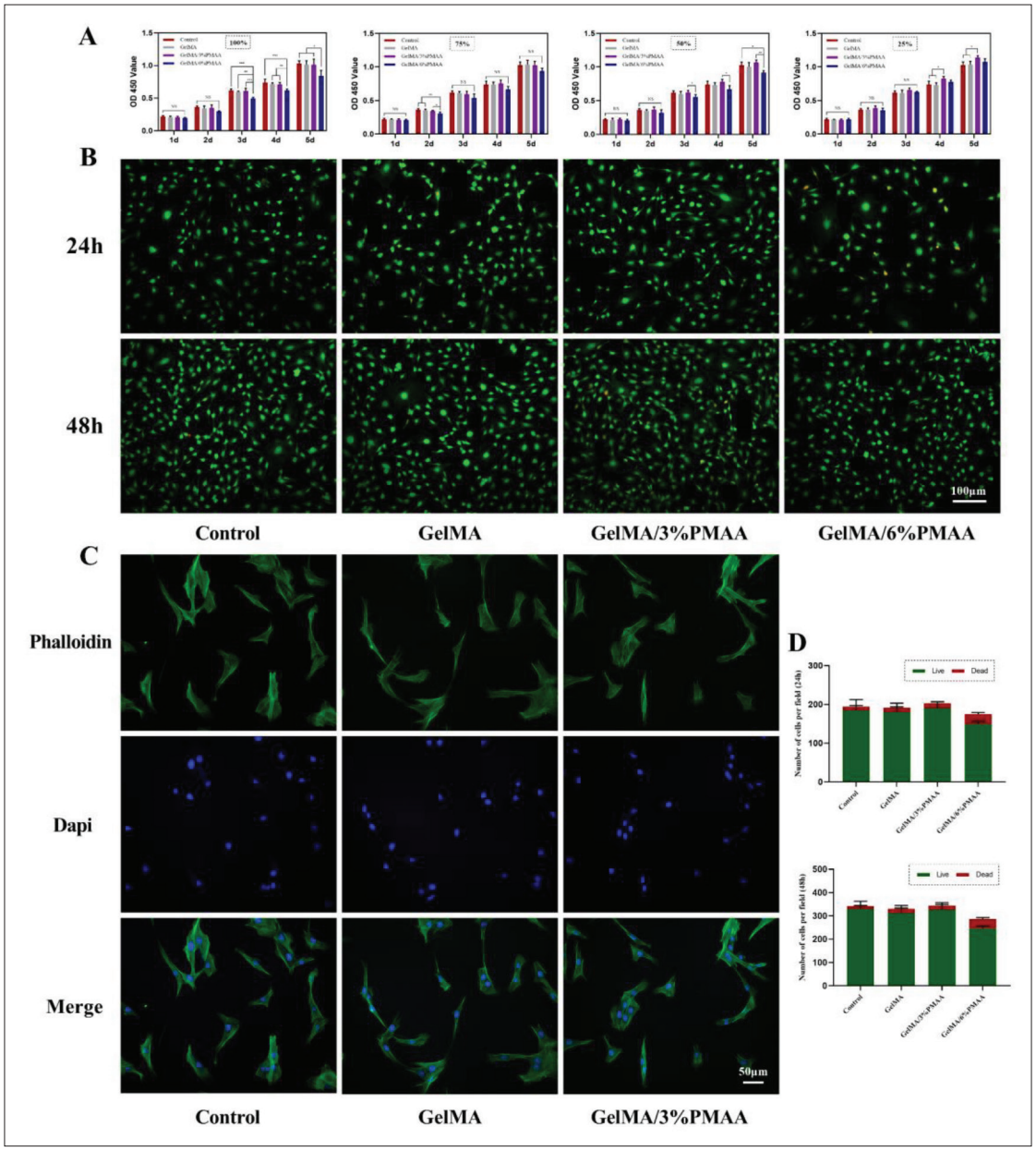


**Figure 3**. Biocompatibility of GelMA/PMAA scaffold *in vitro*. (A) CCK-8 assay showing the proliferation of BMSCs after co-cultured with different extracts of different scaffolds for 1–5 days. (B) Live/dead assay of BMSCs co-cultured with 25% extract; green represents living cells and red represents dead cells. (C) Phalloidin assay of BMSCs co-cultured with 25% extract. (D) Number of cells in live/dead assay. Data were analyzed via one-way ANOVA and are shown as mean ± standard deviation (*$p < 0.05$, **$p < 0.01$, ***$p < 0.001$, $n = 3$).

of PMAA (Figure 3A). Therefore, the extract with 25% of concentration was selected for the next immunofluorescence staining. Live/dead staining showed a poor proliferation of cells cultured in the GelMA/6% PMAA extract (Figure 3B and D). In contrast, the morphology and proliferation of the cells were not significantly affected by the extract of GelMA/3%PMAA (Figure 3C). The cells on either GelMA or GelMA/3% PMAA scaffold showed high viability after 24 h of inoculation on the scaffold surface (**Figure S2** in Supplementary File). Therefore, GelMA/3%PMAA is a more suitable bio-ink.

### 3.3. Expression of HIF-1α after chelation of iron ions

In hypoxic environments, a series of reactive behaviors are performed by cells, such as elevation of HIF-1α, a signal molecule that senses oxygen, which subsequently triggers a series of biological effects. As shown in Figure 4A, it could be found that GelMA/3%PMAA hydrogel possessed the

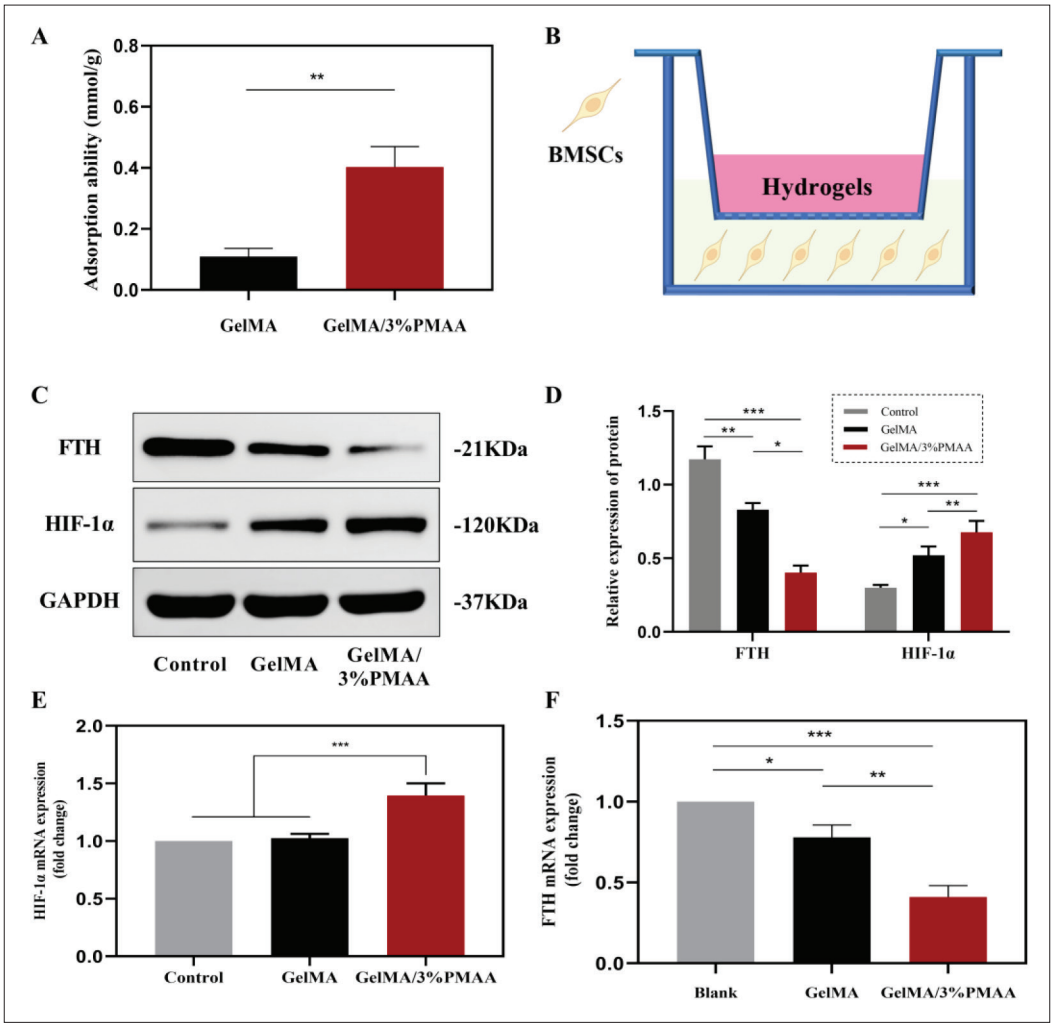


**Figure 4**. Expression of HIF-1α and ability of chelating iron ions. (A) Iron ion chelation of GelMA, GelMA/3%PMAA scaffolds in $FeCl_3$ solution. (B) Schematic of effect of scaffolds on BMSCs. (C, D) Protein expression of FTH and HIF-1α in BMSCs using Western blot. (E, F) The gene expression of FTH and HIF-1α in BMSC using quantitative real-time PCR. Data were analyzed via one-way ANOVA and are shown as mean ± standard deviation (*$p < 0.05$, **$p < 0.01$, ***$p < 0.001$, $n = 3$).

ability to chelate iron ions, which was later demonstrated by the reduced ferritin heavy chain (FTH) expression after co-culture with BMSCs (Figure 4C–F). After 5 days of co-culture with GelMA/3%PMAA, it was found that the expression of HIF-1α protein and gene were significantly increased, which was consistent with the results of previous literature that the reduction of iron ions could promote the expression of HIF-1α (Figure 4C–F). These results showed that the GelMA/3%PMAA scaffold could play a role similar to that of a low oxygen environment, providing the basis for ECO.

### 3.4. Capacity for chondrogenic differentiation of BMSCs

It was previously verified that GelMA/3%PMAA hydrogel could chelate iron ions and promote the expression of HIF-1α, which was reported to promote chondrogenic differentiation and chondrocyte proliferation in BMSCs through upregulation of SOX9. After 5 days of co-culture of the hydrogel with BMSCs, the expression of SOX9, a BMSCs-specific transcription factor, was significantly elevated in the GelMA/3% PMAA group, as previously reported in the literature. Aside from that, the expression of the extracellular matrix components COL-II and ACAN was similarly elevated, which also represent the formation of chondrocytes and the secretion of specific extracellular matrix (Figure 5). A similar trend was observed *in vivo* with cartilage production near the scaffold at week 4 versus week 8 (Figure 9), demonstrating that the GelMA/3%PMAA scaffold promoted BMSCs' chondrogenic differentiation and induced ECO initiation.

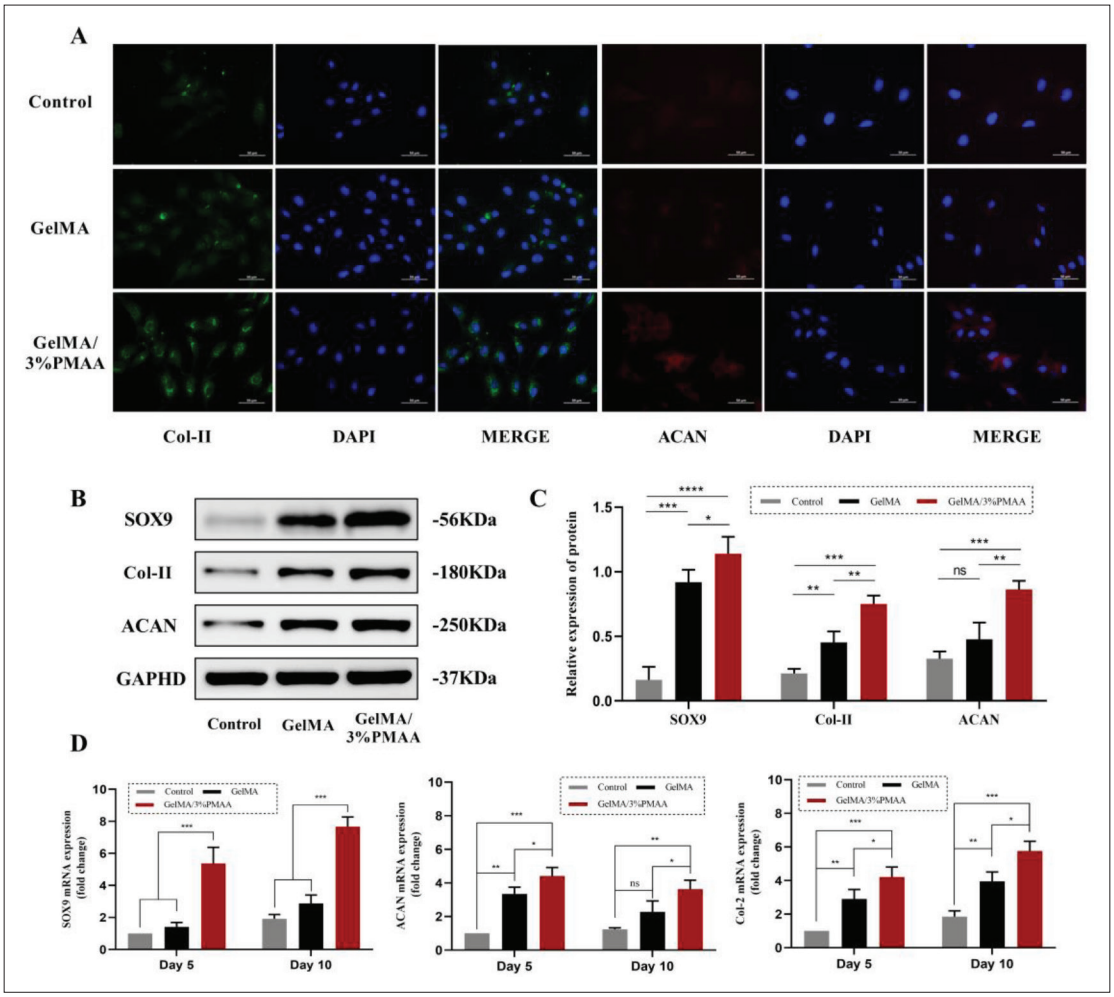


**Figure 5**. Capacity for chondrogenic differentiation of BMSCs. (A) Fluorescent staining of Col-II and ACAN after 5 days of co-culture with scaffolds. (B, C) Protein expression of SOX9, Col-II, and ACAN in BMSCs using Western blot. (D) Gene expression of SOX9, Col-II, and ACAN in BMSCs using quantitative real-time PCR. Data were analyzed via one-way ANOVA and are shown as mean ± standard deviation (*$p < 0.05$, **$p < 0.01$, ***$p < 0.001$, $n = 3$).

### 3.5. Capacity for migration and vascular regeneration of HUVECs

The growth of blood vessels in the ECO process is essential for the mineralization of cartilage templates. Therefore, we investigated the ability of GelMA/3%PMAA hydrogel to promote the migration of HUVECs and the formation of blood vessels. As shown in Figure 6A–D, both transwell and scratch experiments were performed to investigate that the addition of PMAA resulted in better migration of HUVECs. Moreover, *in vitro* tube formation assays also indicated that at 6 h, HUVECs could form more meshes in the presence of PMAA, with longer total length (Figure 6E and F). To investigate the reason, we analyzed the expression of vascular-related factors by co-culturing HUVECs with hydrogel. GelMA/3%PMAA hydrogel was found to promote the protein and mRNA expression of VEGF (Figure 6G and H). The scaffold was then implanted into the defect site of the rabbit femoral condyle bone, where an increase in CD31 of the GelMA/3%PMAA scaffold and an abundance of blood vessels within the new bone tissue were found after 1 month (Figure 8). This indicated that the GelMA/3%PMAA scaffold promoted vascular regeneration at the defect site that was important for the mineralization of cartilage templates during ECO.

### 3.6. Initiation of ECO *in vivo*

To verify the early results of different scaffolds for the treatment of bone defects, we implanted them in rabbit femoral condylar defects and analyzed them using micro-CT, which revealed that at week 4 and week 8, GelMA/3%PMAA scaffolds achieved better efficacy compared to other groups in both BMD, BV/TV, Th.Tb, and Th.Sp (Figure 7). We then analyzed the vascular regeneration at the defect site at week 4 and found increased CD31 in GelMA/3%PMAA scaffolds as well as abundant vascularity within the new bone tissue, while no significant new bone was present around the GelMA

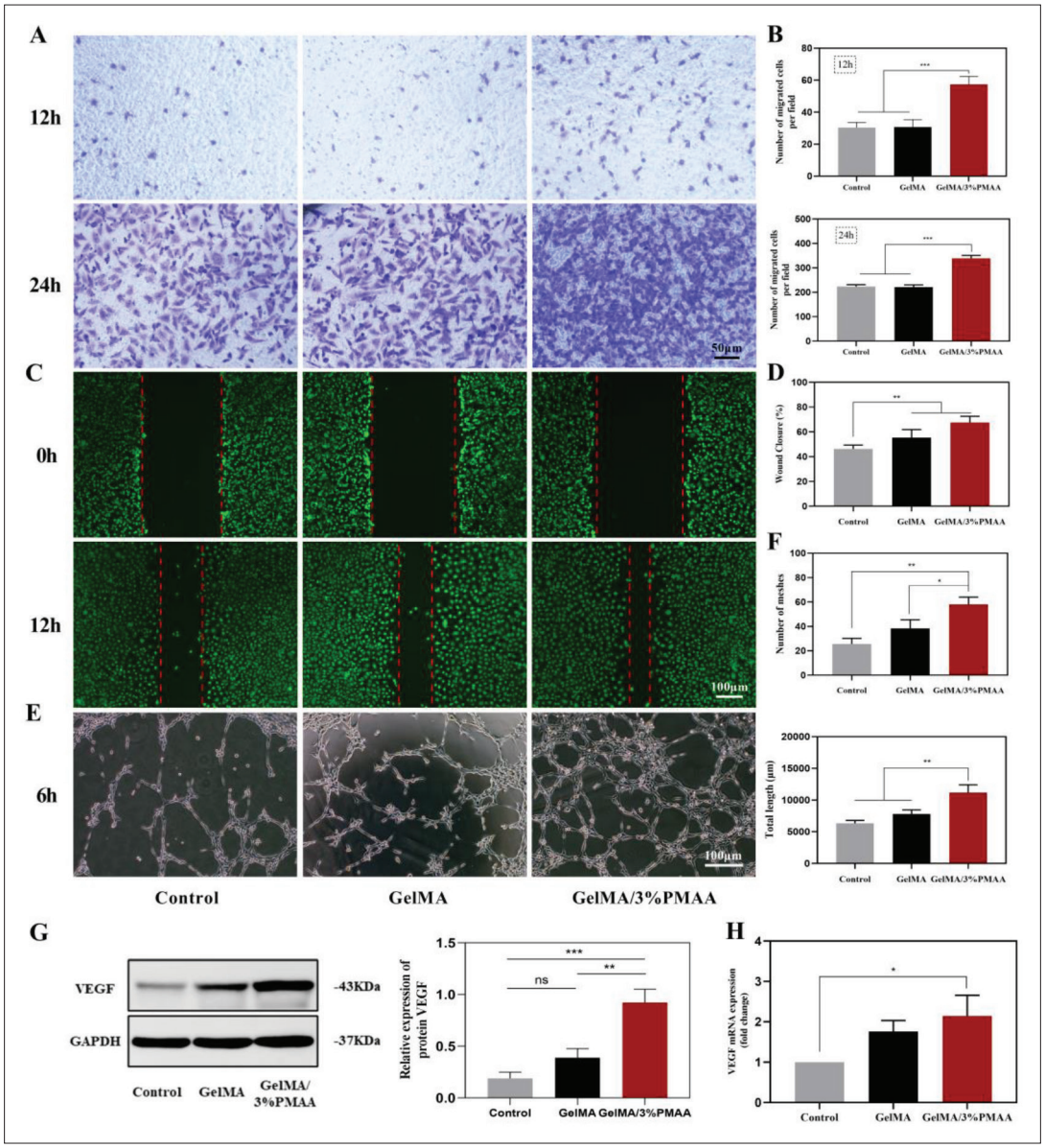


**Figure 6**. Capacity for migration and vascular regeneration of HUVECs. (A, B) Transwell assay at 12 h and 24 h. (C, D) Migration experiment of scratch wound assay at 12 h and quantitative results of wound closure. (E, F) The endothelial tube formation in HUVECs at 6 h after culturing with different scaffolds and summarized data of total length and number of meshes. (G) Protein expression VEGF in HUVECs using Western blot. (H) Gene expression of VEGF in HUVECs using quantitative real-time PCR. Data were analyzed via one-way ANOVA and are shown as mean ± standard deviation (*$p < 0.05$, **$p < 0.01$, ***$p < 0.001$, $n = 3$).

scaffolds despite the presence of neovascularization (Figure 8). Additionally, the hematoxylin–eosin staining and Masson's trichrome staining of tissues at week 4 and week 8 revealed a large amount of cartilage tissue near the GelMA/3%PMAA scaffold and surrounding mineralized bone enriched with blood vessels, whereas no cartilage was observed surrounding the GelMA scaffolds (Figure 9). Sirius red staining also revealed that more new bone could be observed in the GelMA/3%PMAA scaffold compared to the GelMA scaffold, while the new bone showed a reticular structure similar to that of the scaffold (**Figure S3** in Supplementary File). In summary, it was demonstrated that GelMA/3%PMAA hydrogel scaffold could chelate iron ions and induce the classical ECO pathway by upregulating the expression of HIF-1α in order to complete bone tissue regeneration.

## 4. Discussion

In the last decades, significant progress has been achieved in the development of artificial bone-substitute materials[45].

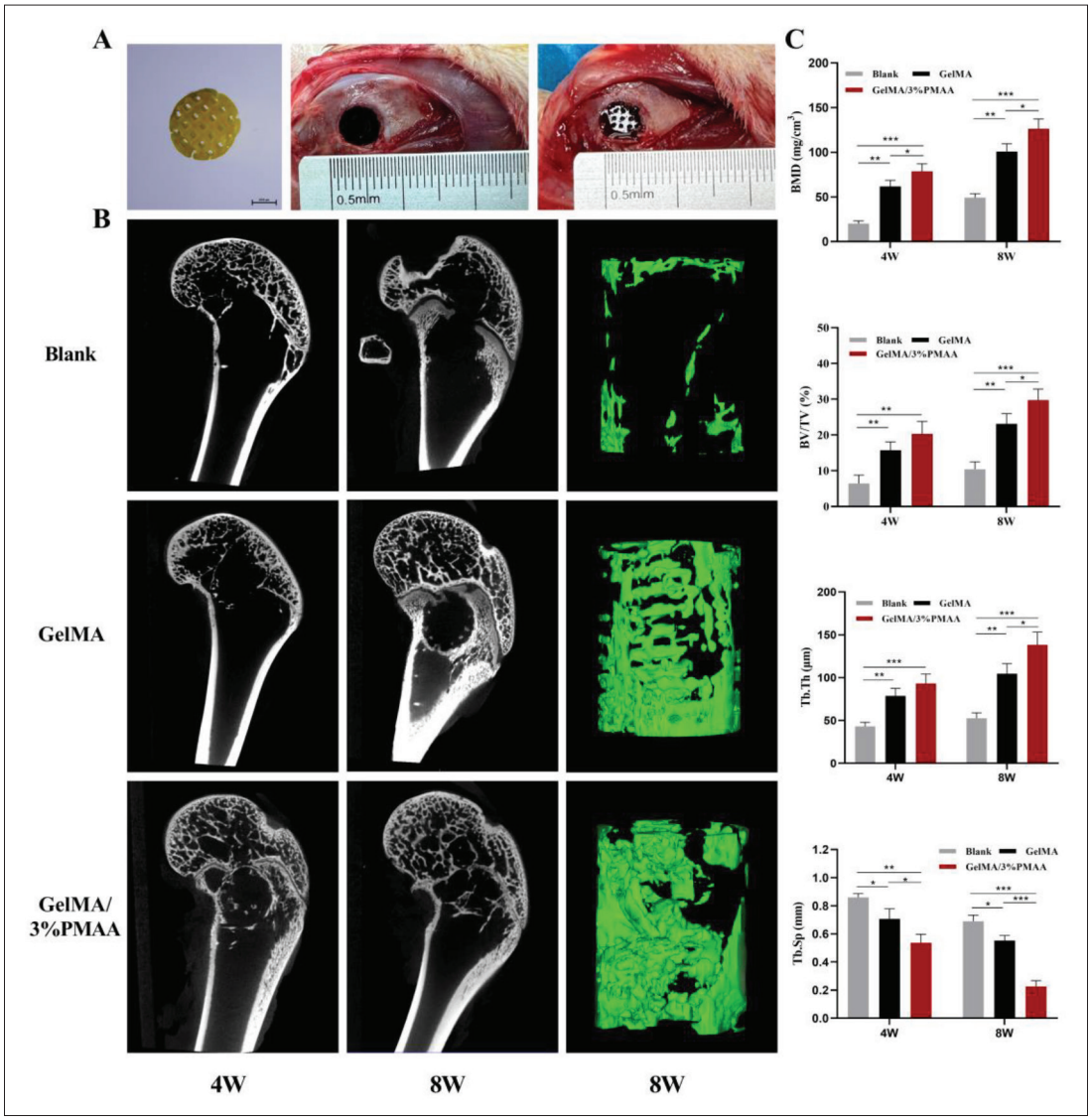


**Figure 7**. Micro-CT analysis of new bone formation at week 4 (4W) and week 8 (8W). (A) Images of the scaffold and its implantation into the defect site of femoral condyle. (B) Micro-CT images at week 4 and week 8 with the reconstructed images of femur defects at week 8. (C) The micro-architectural parameters of newly formed bone. (BMD, bone mineral density; BV/TV, bone tissue volume/total tissue volume; Tb.Th, trabecular thickness; Tb.Sp, trabecular separation). Data were analyzed via one-way ANOVA and are shown as mean ± standard deviation (*$p < 0.05$, **$p < 0.01$, ***$p < 0.001$, $n = 3$).

With different compositions and structures, the bone-substitute materials are endowed with diverse biological activities during different phases of bone regeneration under various environments[30,36,45-49].

IMO and ECO are two forms of bone regeneration[3-6], in which ECO has been shown to be a natural way of bone formation in embryonic period and one of the ways by which bone regenerates during fracture healing[12-14]. The ECO approach to bone regeneration is currently attracting more and more attention from researchers. Several studies have shown that certain growth factors can induce ECO, such as HIF-1α, which regulates the behavior of chondrocytes and activates vascular regeneration[23,24,26]. Although growth factors are effective in inducing ECO, the problems such as high cost, low activity, and potential side effects of growth factors remain unresolved. Some drugs, such as DFO, have likewise been used to promote the expression of HIF-1α. Zhang *et al.* reported that a biomimetically hierarchical scaffold composed of deferoxamine@poly(ε-caprolactone) nanoparticles (DFO@PCL NPs), manganese carbonyl (MnCO) nanosheets, gelatin methacryloyl hydrogel, and a polylactide/hydroxyapatite matrix was fabricated to augment bone repair by facilitating the angiogenesis and bone metabolism. However, the explosive release of exogenous drugs poses a significant biosafety risk[30].

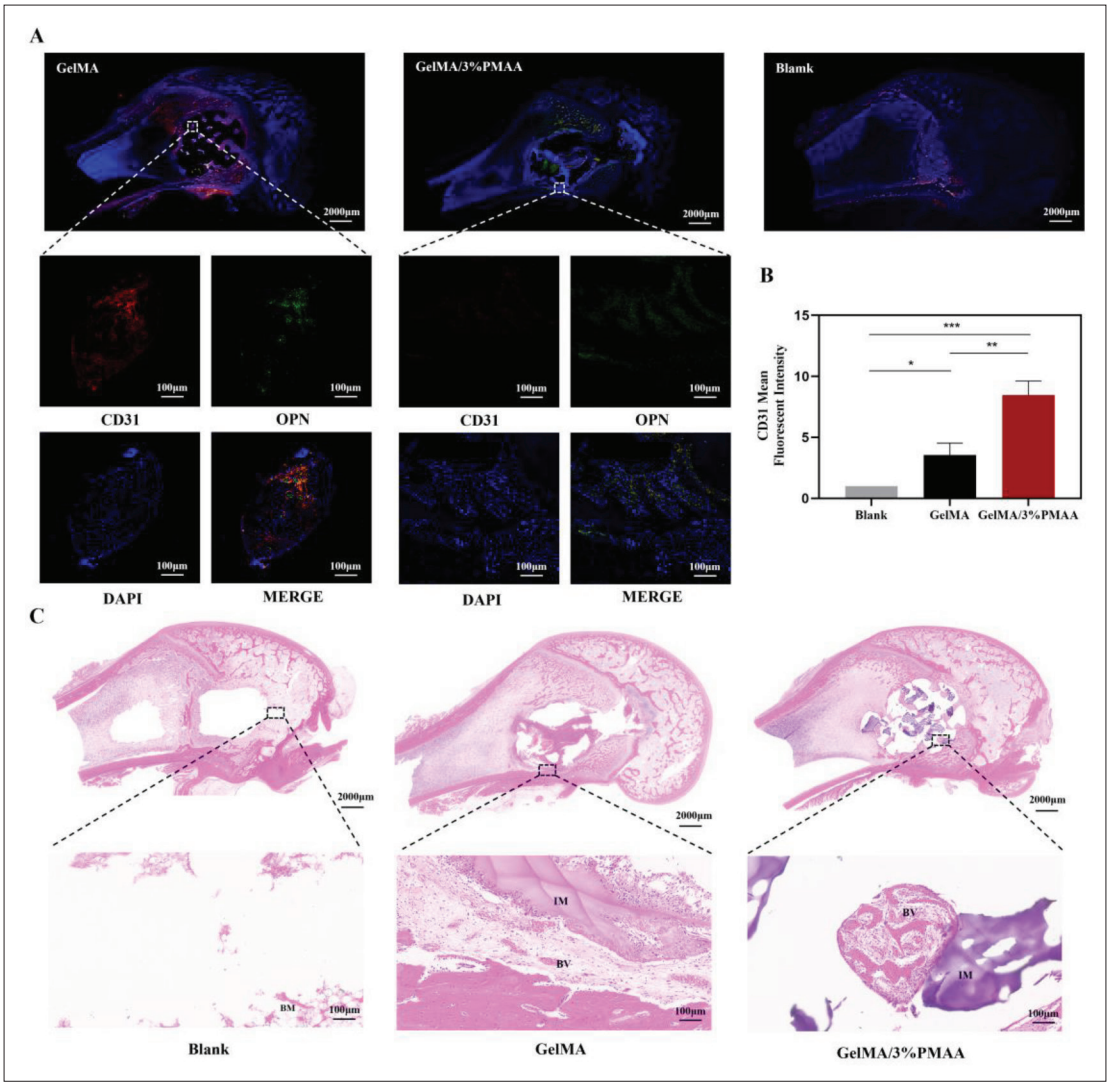


**Figure 8**. Histological and immunohistochemistry evaluation of the new blood vessels in the defect site at week 4. (A) Fluorescent staining (CD31 and OPN) of newly formed bone at week 4. (B) The mean fluorescent intensity of CD31. (C) Hematoxylin–eosin staining of newly formed bone at week 4. Data were analyzed using one-way ANOVA and are shown as mean ± standard deviation (*$p < 0.05$, **$p < 0.01$, ***$p < 0.001$, $n = 3$). (NB, new bone; IM, implanted materials; BM, bone marrow; BV, blood vessel.)

Therefore, it has become an attractive strategy to induce ECO *in situ* through the properties of the material itself[50]. Sun *et al.* prepared an injectable, poly (glycerol sebacate)-co-poly (ethylene glycol)/polyacrylic acid (PEGS/PAA) hydrogels to induce a hypoxia-mimicking environment and subsequently recapitulate ECO via *in situ* iron chelation[37]. However, injectable hydrogels cannot be prepared directly as pre-designed macroscopic structures.

In our study, GelMA/PMAA scaffolds promoted the expression of HIF-1α by chelating iron ions with the carboxyl group of PMAA, thus reducing the consumption of HIF-1α by PHD and allowing for better chondrocyte differentiation and vascular regeneration. The scaffolds also overcame the disadvantages of exogenous factors and allowed smooth progression of ECO. Furthermore, owing to their excellent structure, the 3D-printed scaffold also supported the access of bone tissue and blood vessels, providing a novel material design for ECO-based bone regeneration.

The GelMA/PMAA scaffold possessed better elasticity and compression strength compared to the conventional GelMA scaffold, increasing early mechanical stability and meeting the mechanical requirements of inclusive bone defects. In terms of surface structure, the 3D printing technology could help the scaffold to achieve the co-existence of macropores and micropores, as compared to only micropores in the conventional injectable hydrogel, which is essential for the occurrence of osteoconductivity. In addition, the introduction of PMAA not only improved

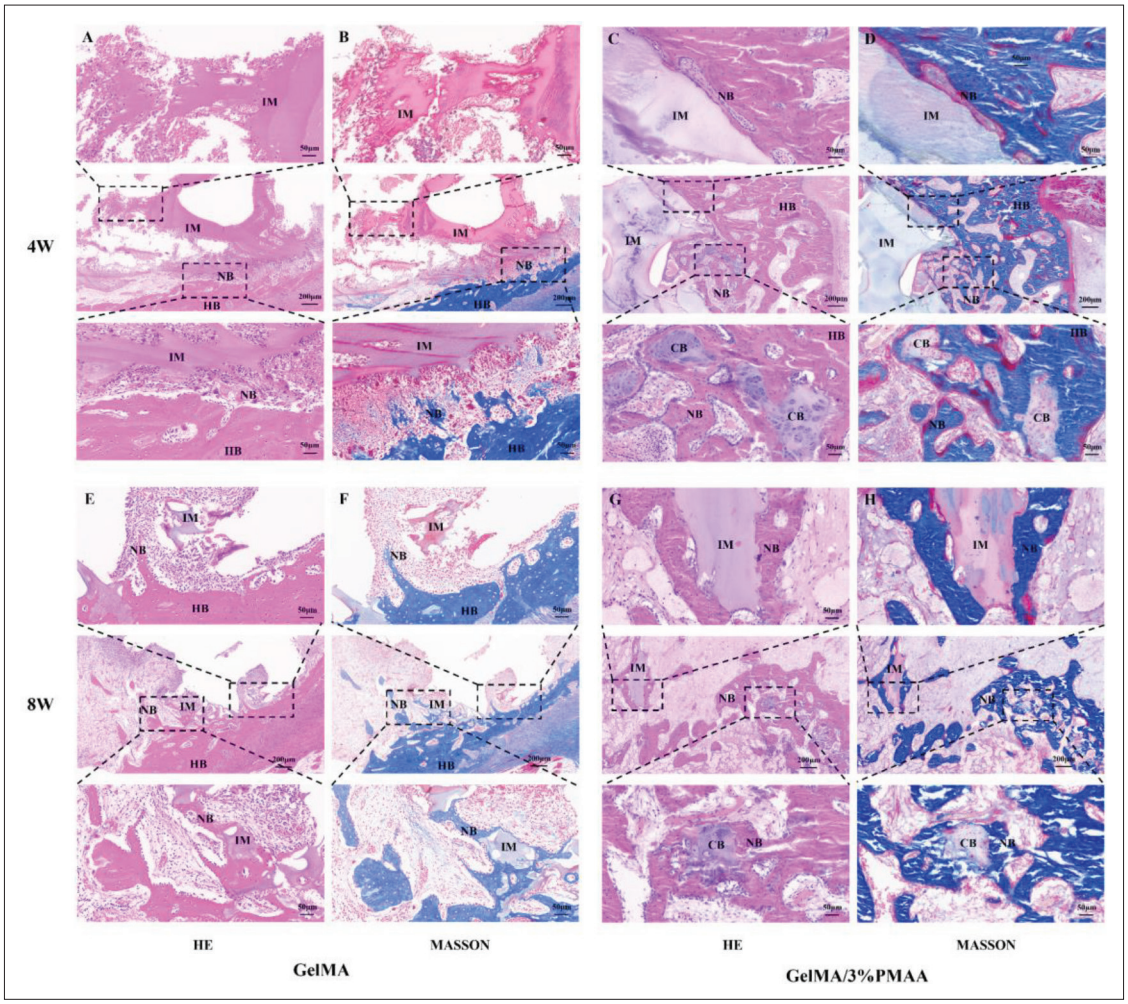


**Figure 9**. Histological evaluation of newly formed bone at week 4 and week 8. (A, C) Hematoxylin–eosin (HE) and (B, D) Masson's trichrome (MASSON) staining in the defect site at week 4. (E, G) HE and (F, H) MASSON staining in the defect site at week 8. (NB, new bone; HB, host bone; IM, implanted materials; CB, chondrogenic bone.)

3D printing accuracy, but the good anti-swelling property also helps to better maintain the pore structure, and the extended degradation time matches the rate of bone regeneration (Figure 2).

*In vitro* and *in vivo* bioeffects studies verified the chelation iron ions in the material by ICP, Western blot, and PCR, and also confirmed that GelMA/3%PMAA promotes the expression of HIF-1α as expected, which was crucial for our next studies (Figure 4). As previously mentioned, two vital points for ECO are the chondrogenic differentiation of BMSCs and the regeneration of blood vessels. After co-cultured with GelMA/3%PMAA, the expression of SOX9 as well as the secretion of extracellular matrix components, such as COL-II and ACAN, was improved, indicating the differentiation of BMSCs to cartilage. In contrast, only a small amount of SOX9 expression was observed in GelMA hydrogel (Figure 5). In combination with histological examination, it was also found that some chondrocyte aggregation was observed around the GelMA/3%PMAA hydrogel, regardless of week 4 or week 8, with mineralized bone tissue appearing "in the surrounding" (Figure 9). It was demonstrated that GelMA/3%PMAA scaffold could effectively promote chondrogenic differentiation of BMSCs, which is vital for the induction of ECO.

Vascular regeneration is crucial for ECO, without timely vascular invasion, and ECO will stagnate in the cartilage template and fail to mineralize into bone. GelMA/3%PMAA played a non-negligible role in angiogenesis by promoting cartilage differentiation while also upregulating HIF-1α, promoting HUVECs migration and VEGF expression (Figure 6). In addition, the histological staining showed that more blood vessels were formed in the GelMA/3%PMAA hydrogel group at week 4, accompanied by more Osteopontin (OPN) expression.

Combined with the mineralization and osteogenesis of cartilage at week 4 and week 8, the adsorption of iron ions and the abundant expression of HIF-1α resulted in a good balance between cartilage and bone due to the growth of blood vessels into the bone (Figures 8 and 9). Thus, the GelMA/3%PMAA hydrogel well induced the process of ECO and promoted the regeneration of bone.

In this study, GelMA/3%PMAA scaffolds with porous structure were prepared using DLP printing technology, which could further promote chondrogenic differentiation of BMSCs and vascular regeneration by chelating iron ions to promote the expression of HIF-1α without the help of exogenous factors. GelMA/3%PMAA scaffolds could induce ECO through their own properties to regulate bone regeneration, providing a new approach for clinical treatment of bone defects, especially non-weight-bearing bone defects manifesting weak angiogenesis.

## 5. Conclusion

In conclusion, a biocompatible GelMA/PMAA scaffold was successfully developed to recapitulate and accelerate *in situ* ECO-based bone regeneration through increasing HIF-1α by adsorption of iron ions while ensuring structural advantages to induce cartilage differentiation and vascular regeneration. The ability to realize ECO through the properties of materials via biomaterial-based iron ion chelation provides a promising strategy for clinical treatment of bone defects.

## Acknowledgments

We thank Institute of Orthopedics, PLA General Hospital, for providing the experimental equipment.

## Funding

This work was supported by the Key Program of the National Natural Science Foundation of China (grant number 21935011), the Beijing Municipal Natural Science Foundation (grant number L202033), and the Military Medical Science and Technology Youth Training Program (grant number 19QNP052).

## Conflict of interest

The authors declare no conflict of interest.

## Author contributions

*Conceptualization:* Jianpeng Gao, Hufei Wang
*Formal analysis:* Jianheng Liu, Ming Li
*Funding acquisition:* Xing Wang, Jianheng Liu
*Investigation:* Jianpeng Gao, Hufei Wang, Jianheng Liu
*Methodology:* Licheng Zhang, Xing Wang
*Resources:* Licheng Zhang, Xing Wang
*Validation:* Zhongyang Liu, Junyao Cheng, Xiao Liu
*Writing – original draft:* Jianpeng Gao, Hufei Wang
*Writing – review & editing:* Jianheng Liu, Xing Wang, Licheng Zhang

## Ethics approval and consent to participate

The Institutional Animal Care and Use Committee of the Chinese PLA General Hospital approved the design of this study (2022-x18-51).

## Consent for publication

Not applicable.

## Availability of data

The datasets used and analyzed during the current study are available from the corresponding author on reasonable request.

## References

1. Gillman CE, Jayasuriya AC, 2021, FDA-approved bone grafts and bone graft substitute devices in bone regeneration. *Mater Sci Eng C Mater Biol Appl,* 130: 112466.

   https://doi.org/10.1016/j.msec.2021.112466

2. Bose S, Sarkar N, 2020, Natural medicinal compounds in bone tissue engineering. *Trends Biotechnol,* 38(4): 404–417.

   https://doi.org/10.1016/j.tibtech.2019.11.005

3. Ghimire S, Miramini S, Edwards G, *et al.*, 2021, The investigation of bone fracture healing under intramembranous and endochondral ossification. *Bone Rep,* 14: 100740.

   https://doi.org/10.1016/j.bonr.2020.100740

4. Galea GL, Zein MR, Allen S, *et al.*, 2021, Making and shaping endochondral and intramembranous bosnes. *Dev Dyn,* 250(3): 414–449.

   https://doi.org/10.1002/dvdy.278

5. Chan WCW, Tan Z, To MKT, *et al.*, 2021, Regulation and role of transcription factors in osteogenesis. *I J Mol Sci,* 22(11): 5445.

   https://doi.org/10.3390/ijms22115445

6. Weng Y, Wang H, Wu D, *et al.*, 2022, A novel lineage of osteoprogenitor cells with dual epithelial and mesenchymal properties govern maxillofacial bone homeostasis and regeneration after MSFL. *Cell Res,* 32(9): 814–830.

   https://doi.org/10.1038/s41422-022-00687-x

7. He J, Yan J, Wang J, *et al.*, 2021, Dissecting human embryonic skeletal stem cell ontogeny by single-cell transcriptomic and functional analyses. *Cell Res,* 31(7): 742–757.

   https://doi.org/10.1038/s41422-021-00467-z

8. Siddiqui Z, Sarkar B, Kim KK, *et al.*, 2021, Self-assembling peptide hydrogels facilitate vascularization in two-component scaffolds. *Chem Eng J,* 422: 130145.

   https://doi.org/10.1016/j.cej.2021.130145

9. Bernhard JC, Marolt Presen D, Li M, *et al.*, 2022, Effects of endochondral and intramembranous ossification pathways on bone tissue formation and vascularization in human tissue-engineered grafts. *Cells,* 11(19): 3070.

   https://doi.org/10.3390/cells11193070

10. Saul D, Khosla S, 2022, Fracture healing in the setting of endocrine diseases, aging, and cellular senescence. *Endocr Rev,* 43(6): 984–1002.

    https://doi.org/10.1210/endrev/bnac008

11. Ye X, He J, Wang S, *et al.*, 2022, A hierarchical vascularized engineered bone inspired by intramembranous ossification for mandibular regeneration. *Int J Oral Sci,* 14(1): 31.

    https://doi.org/10.1038/s41368-022-00179-z

12. Fernández-Iglesias Á, Fuente R, Gil-Peña H, *et al.*, 2021, The formation of the epiphyseal bone plate occurs via combined endochondral and intramembranous-like ossification. *Int J Mol Sci,* 22(2): 900.

    https://doi.org/10.3390/ijms22020900

13. Fu R, Liu C, Yan Y, *et al.*, 2021, Bone defect reconstruction via endochondral ossification: A developmental engineering strategy. *J Tissue Eng,* 12: 20417314211004211.

    https://doi.org/10.1177/20417314211004211

14. Liu Y, Yang Z, Wang L, *et al.*, 2021, Spatiotemporal immunomodulation using biomimetic scaffold promotes endochondral ossification-mediated bone healing. *Adv Sci,* 8(11): e2100143.

    https://doi.org/10.1002/advs.202100143

15. Wu L, Gu Y, Liu L, *et al.*, 2020, Hierarchical micro/nanofibrous membranes of sustained releasing VEGF for periosteal regeneration. *Biomaterials,* 227: 119555.

    https://doi.org/10.1016/j.biomaterials.2019.119555

16. Peng K, Zhuo M, Li M, *et al.*, 2020, Histone demethylase JMJD2D activates HIF1 signaling pathway via multiple mechanisms to promote colorectal cancer glycolysis and progression. *Oncogene,* 39(47): 7076–7091.

    https://doi.org/10.1038/s41388-020-01483-w

17. Zhang S, Wang Y, Xu J, *et al.*, 2021, HIFα regulates developmental myelination independent of autocrine Wnt signaling. *J Neurosci,* 41(2): 251–268.

    https://doi.org/10.1523/jneurosci.0731-20.2020

18. Wang P, Xiong X, Zhang J, *et al.*, 2020, Icariin increases chondrocyte vitality by promoting hypoxia-inducible factor-1α expression and anaerobic glycolysis, *Knee,* 27(1): 18–25.

    https://doi.org/10.1016/j.knee.2019.09.012

19. Fujii Y, Liu L, Yagasaki L, *et al.*, 2022, Cartilage homeostasis and osteoarthritis. *Int J Mol Sci,* 23(11): 6316.

    https://doi.org/10.3390/ijms23116316

20. Ito Y, Matsuzaki T, Ayabe F, *et al.*, 2021, Both microRNA-455-5p and -3p repress hypoxia-inducible factor-2α expression and coordinately regulate cartilage homeostasis, *Nat Commun,* 12(1): 4148.

    https://doi.org/10.1038/s41467-021-24460-7

21. Jouan Y, Bouchemla Z, Bardèche-Trystram B, *et al.*, 2022, Lin28a induces SOX9 and chondrocyte reprogramming via HMGA2 and blunts cartilage loss in mice. *Sci Adv,* 8(34): eabn3106.

    https://doi.org/10.1126/sciadv.abn3106

22. Haseeb A, Kc R, Angelozzi M, *et al.*, 2021, SOX9 keeps growth plates and articular cartilage healthy by inhibiting chondrocyte dedifferentiation/osteoblastic redifferentiation. *Proc Natl Acad Sci USA,* 118(8): e2019152118.

    https://doi.org/10.1073/pnas.2019152118

23. Maes C, Carmeliet G, Schipani E, 2012, Hypoxia-driven pathways in bone development, regeneration and disease. *Nat Rev Rheumatol,* 8(6): 358–366.

    https://doi.org/10.1038/nrrheum.2012.36

24. Solanki AK, Lali FV, Autefage H, *et al.*, 2021, Bioactive glasses and electrospun composites that release cobalt to stimulate the HIF pathway for wound healing applications. *Biomater Res,* 25(1): 1.

    https://doi.org/10.1186/s40824-020-00202-6

25. Peng Y, Wu S, Li Y, *et al.*, 2020, Type H blood vessels in bone modeling and remodeling. *Theranostics,* 10(1): 426–436.

    https://doi.org/10.7150/thno.34126

26. Wan C, Gilbert SR, Wang Y, *et al.*, 2008, Activation of the hypoxia-inducible factor-1alpha pathway accelerates bone regeneration. *Proc Natl Acad Sci USA,* 105(2): 686–691.

    https://doi.org/10.1073/pnas.0708474105

27. Voit RA, Sankaran VG, 2020, Stabilizing HIF to ameliorate anemia. *Cell,* 180: 6(1).

    https://doi.org/10.1016/j.cell.2019.12.010

28. Kaelin WG, Jr., Ratcliffe PJ, 2008, Oxygen sensing by metazoans: the central role of the HIF hydroxylase pathway. *Mol Cell,* 30(4): 393–402.

    https://doi.org/10.1016/j.molcel.2008.04.009

29. Zheng X, Zhang X, Wang Y, *et al.*, 2021, Hypoxia-mimicking 3D bioglass-nanoclay scaffolds promote endogenous bone regeneration. *Bioact Mater,* 6(10): 3485–3495.

    https://doi.org/10.1016/j.bioactmat.2021.03.011

30. Zhang J, Tong D, Song H, *et al.*, 2022, Osteoimmunity-regulating biomimetically hierarchical scaffold for augmented bone regeneration. *Adv Mater,* 34(36): e2202044.

    https://doi.org/10.1002/adma.202202044

31. Cui J, Yu X, Yu B, *et al.*, 2022, Coaxially fabricated dual-drug loading electrospinning fibrous mat with programmed releasing behavior to boost vascularized bone regeneration. *Adv Healthc Mater,* 11(16): e2200571.

    https://doi.org/10.1002/adhm.202200571

32. Han X, Sun M, Chen B, *et al.*, 2021, Lotus seedpod-inspired internal vascularized 3D printed scaffold for bone tissue repair. *Bioact Mater,* 6(6): 1639–1652.

    https://doi.org/10.1016/j.bioactmat.2020.11.019

33. Donneys A, Yang Q, Forrest ML, *et al.*, 2019, Implantable hyaluronic acid-deferoxamine conjugate prevents nonunions through stimulation of neovascularization. *NPJ Regen Med,* 4: 11.

    https://doi.org/10.1038/s41536-019-0072-9

34. Yao Q, Liu Y, Selvaratnam B, *et al.*, 2018, Mesoporous silicate nanoparticles/3D nanofibrous scaffold-mediated dual-drug delivery for bone tissue engineering. *J Control Release,* 279: 69–78.

    https://doi.org/10.1016/j.jconrel.2018.04.011

35. Drager J, Sheikh Z, Zhang YL, *et al.*, 2016, Local delivery of iron chelators reduces in vivo remodeling of a calcium phosphate bone graft substitute. *Acta Biomater,* 42: 411–419.

    https://doi.org/10.1016/j.actbio.2016.07.037

36. Liu Z, Zhang J, Fu C, *et al.*, 2023, Osteoimmunity-regulating biomaterials promote bone regeneration. *Asian J Pharm Sci,* 18(1): 100774.

    https://doi.org/10.1016/j.ajps.2023.100774

37. Sun LL, Ma YF, Niu HY, *et al.*, 2021, Recapitulation of in situ endochondral ossification using an injectable hypoxia-mimetic hydrogel. *Adv Funct Mater,* 31(5).

    https://doi.org/10.1002/adfm.202008515

38. Chen YC, Lin RZ, Qi H, *et al.*, 2012, Functional human vascular network generated in photocrosslinkable gelatin methacrylate hydrogels. *Adv Funct Mater,* 22(10): 2027–2039.

    https://doi.org/10.1002/adfm.201101662

39. Schuurman W, Levett PA, Pot MW, *et al.*, 2013, Gelatin-methacrylamide hydrogels as potential biomaterials for fabrication of tissue-engineered cartilage constructs. *Macromol Biosci,* 13(5): 551–561.

    https://doi.org/10.1002/mabi.201200471

40. Kurian AG, Singh RK, Patel KD, *et al.*, 2022, Multifunctional GelMA platforms with nanomaterials for advanced tissue therapeutics. *Bioact Mater,* 8: 267–295.

    https://doi.org/10.1016/j.bioactmat.2021.06.027

41. Hong Y, Zhou F, Hua Y, *et al.*, 2019, A strongly adhesive hemostatic hydrogel for the repair of arterial and heart bleeds. *Nat Commun,* 10(1): 2060.

    https://doi.org/10.1038/s41467-019-10004-7

42. Gao Q, Niu X, Shao L, *et al.*, 2019, 3D printing of complex GelMA-based scaffolds with nanoclay. *Biofabrication,* 11(3): 035006.

    https://doi.org/10.1088/1758-5090/ab0cf6

43. Ratheesh G, Vaquette C, Xiao Y, 2020, Patient-specific bone particles bioprinting for bone tissue engineering. *Adv Healthc Mater,* 9(23): e2001323.

    https://doi.org/10.1002/adhm.202001323

44. Gao J, Ding X, Yu X, *et al.*, 2021, Cell-free bilayered porous scaffolds for osteochondral regeneration fabricated by continuous 3D-printing using nascent physical hydrogel as ink. *Adv Healthc Mater,* 10(3): e2001404.

    https://doi.org/10.1002/adhm.202001404

45. Zhu T, Cui Y, Zhang M, *et al.*, 2020, Engineered three-dimensional scaffolds for enhanced bone regeneration in osteonecrosis. *Bioact Mater,* 5(3): 584–601.

    https://doi.org/10.1016/j.bioactmat.2020.04.008

46. Zhu T, Jiang M, Zhang M, *et al.*, 2022, Construction and validation of steroid-induced rabbit osteonecrosis model. *MethodsX,* 9: 101713.

    https://doi.org/10.1016/j.mex.2022.101713

47. Zhu T, Jiang M, Zhang M, *et al.*, 2022, Biofunctionalized composite scaffold to potentiate osteoconduction, angiogenesis, and favorable metabolic microenvironment for osteonecrosis therapy. *Bioact Mater,* 9: 446–460.

    https://doi.org/10.1016/j.bioactmat.2021.08.005

48. Zhao D, Zhu T, Li J, *et al.*, 2021, Poly(lactic-co-glycolic acid)-based composite bone-substitute materials. *Bioact Mater,* 6 (2): 346–360.

    https://doi.org/10.1016/j.bioactmat.2020.08.016

49. Cui L, Zhang J, Zou J, *et al.*, 2020, Electroactive composite scaffold with locally expressed osteoinductive factor for synergistic bone repair upon electrical stimulation. *Biomaterials,* 230: 119617.

    https://doi.org/10.1016/j.biomaterials.2019.119617

50. Sun LL, Ma YF, Niu HY, *et al.*, 2021, Recapitulation of in situ endochondral ossification using an injectable hypoxia-mimetic hydrogel. *Adv Funct Mater,* 31(5): 2008515.

    https://doi.org/10.1002/adfm.202101589